INTERACTIVE AIRCRAFT FLIGHT CONTROL AND

AEROELASTIC STABILIZATION

NASA/Langley Research Center Grant-NAG-1-157

Semi-annual Report

1 May 1985 through 31 October 1985

Submitted by:

Dr. Terrence A. Weisshaar

Principal Investigator

SCHOOL OF AERONAUTICS AND ASTRONAUTICS

PURDUE UNIVERSITY

WEST LAFAYETTE, INDIANA   47907

November 1985

1.0 Summary

This report covers activity during the time period 1 May 1985 through 31 October 1985. During this time one faculty member and two graduate students were supported by this grant. One student, Mr. James Sallee spent 10 weeks in-residence at NASA Langley as part of his gradu ate training. A second student, Mr. Thomas Zeiler received his Ph.D. degree from Purdue in August 1985. His graduate dissertation was sponsored by the Grant. The Principal Investigator spent one week in-residence at NASA/Langley during June 1985. In addition, he presented a talk at the Aerospace Flutter and Dynamics Council Semi-annual meeting in Atlantic City, New Jersey in October 1985. A portion of Mr. Zeiler's dissertation work has been submitted for consideration for the AIAA SDM Meeting to be held in San Antonio, Texas in May 1986.

This report briefly describes research completed by Dr. Zeiler and Professor Weisshaar. A copy of Dr. Zeiler's dissertation has been forwarded to the contract monitor. The proposal for the SDM paper is contained in the Appendix. In addition, the preliminary work by Mr. Sallee and Professor Weisshaar is discussed. A detailed exposition of that work is also contained in the Appendix.

2.0 Aeroservoelastic Optimization Studies

A preliminary study of aeroservoelastic optimization techniques was completed in August 1985. The objective of this study was to determine a methodology for maximization of the stable flight envelope of an idealized, actively controlled, flexible airfoil. The equations of motion for the airfoil were developed in state-space form to include time-domain representations of aerodynamic forces and active control. For optimization, the shear center position was taken to be a design variable. Optimal, steady-state, linear-quadratic regulator theory (SSLQR) was used for control law synthesis.

The synthesis of feedback control laws with SSLQR theory can present problems. One recurring problem is that a system may be stabilized actively at a certain design airspeed (or a nondimensional counterpart, $\overline{U}_{DES}$) but may be unstable at lower, off-design airspeeds. This peculiarity necessitated the development of an optimization scheme to stabilize the aeroelastic system over a range of airspeeds, including the design airspeed. This requirement led to an integrated or multidisciplinary approach that was demonstrated to be beneficial.

Dr. Zeiler organized his solution approach into two levels, one at the "system" level, the other at the "subsystem" level. The subsystems are: (a) the airfoil structure, with a design variable represented by the shear center position; and, (b) the control system. An objective was stated in mathematical form and a search was conducted with the restriction that each subsystem be constrained to be optimal in some sense.

To implement the procedure, analytical expressions were developed to compute the changes in the eigenvalues of the closed-loop, actively controlled system. A stability index was constructed to ensure that

stability was present at the design speed and at other airspeeds away from the design speed.

The design procedure begins with the choice of initial values of shear center position, design airspeed and other control related parameters. A feedback control law is then synthesized and the airspeed envelope is checked for stability by computing the value of the stability index. When the stability index is positive, the system is unstable. The approach relies on a procedure to reduce the value of the stability index below zero (to achieve stability) in an optimal manner. This procedure was demonstrated to be effective. Mathematical results were explained in a physical context.

The above study and the procedure used is described in detail in the Ph.D. dissertation "An Approach to Integrated Aeroservoelastic Tailoring for Stability" by T.A. Zeiler. This study is notable because it indicates a procedure (not the procedure) for a successful iterative structures/control design modification. It has a realistic measure of performance (instability freedom at and within the largest possible design envelope). It also illustrates how one might organize the structural design and control design procedures in a logical way.

3.0   Current Aeroservoelastic Tailoring Studies

The study described in Section 2.0 and the experience gained from those studies has enabled the Principal Investigator to move to the next level of effort. This effort includes a more realistic structural model, incorporating the influence of advanced composite materials. In addition, the effort includes the use of 3-D unsteady aerodynamic effects and classical control procedures (as opposed to optimal control procedures).

This effort is currently in a preliminary stage. As a first step, a highly idealized analytical model has been developed to efficiently include the effect of directional stiffness such as might be present in laminated structures. This model also has educational value as well as research significance. A computer program has also been developed to perform flutter calculations on both the open-loop and closed-lc sys-tems. In addition, the program can compute "sensitivity derivatives" with respect to a variety of system design variables such as stiffness and feedback control gains. These sensitivity derivatives are necessary for system redesign procedures.

The model is also useful as an educational tool to demonstrate to students and professionals the various opportunities afforded by integrated design. The model development has been done by Mr. James Sallee under the direction of Professor Weisshaar. The current status of the analysis and a detailed model description and development is con-tained in the Appendix to this report. This portion of the effort is due for completion at the end of this year. At that time a more detailed, multi-mode analytical model will be implemented to further investigate interesting features revealed by the initial model.

4.0 Future Work

This semi-annual period of the grant has produced results beyond expectation. One Ph.D. student, well-schooled in both control methodology, structural dynamics and aeroelasticity and optimization methods has been graduated and has joined the ranks of American aerospace workers. This event would not have occurred without NASA research sponsorship. The results of the research effort produced by this study are significant and far-reaching. A new student has begun to delve into the subject where the other left off.

The idealization described in the Appendix will be used to survey, in a preliminary manner, several of the more interesting results obtained from Dr. Zeiler's dissertation. In particular, the effects of stiffness cross-coupling on active control are of interest in the current work. An additional difference between the current study and that which preceded it will be the design methodology for the active control itself.

A large portion of the next research period will be spent developing a modal model of a swept wing design. For this study we will attempt to have remote use of ISAC via a Purdue/Langley phone hookup. This effort will be continued with Mr. Sallee in-residence at NASA/Langley, beginning in May 1986.

APPENDIX A

Proposed SDM Presentation

Integrated Aeroservoelastic

Tailoring of Lifting Surfaces

Thomas A. Zeiler*
Kentron International, Inc.
Hampton Technical Center
3221 N. Armistead Ave.
Hampton, Virginia 23666
Phone 804-838-1010

and

-      Terrence A. Weisshaar*
School of Aeronautics and Astronautics
Purdue University
West Lafayette, Indiana 47907
Phone 317-494-5975

*Members, AIAA
 Address all correspondence to the second author.
†Proposed for the Structural Dynamics session.

The design of an aerospace structure involves a complicated sequence of operations requiring multiple, interdisciplinary interactions. The overall design process has a single objective, superior performance subject to a multitude of constraints. Unfortunately, performance has a multiplicity of definitions, depending upon the specific discipline involved within the design process. Worse yet, sometimes these measures of performance are at odds with one another. Future competitive aerospace structural designs will increase the need for creative interaction among the various disciplines and also require accounting for these interactions early in the design process. This paper will discuss the integration of two of these areas, the optimal design process for structures and active control of such a structure. While the results presented are limited in scope, they nonetheless illustrate benefits of integrating the aeroservoelastic design process. This integrated design process is referred to as integrated aeroservoelastic tailoring.

The objective of this study was to determine how to maximize the stable flight envelope of an idealized, actively controlled aeroelastic system shown in Figure 1. This 4-degree-of-freedom system consists of a 3-degree-of-freedom, typical-section airfoil mounted on a rigid support with a stabilizing tail surface; the model is free to pitch about a pivot. This model is intended to simulate a flexible wing with an important body freedom. This model has the potential for simulating high frequency classical flutter behavior, low frequency body-freedom flutter and classical divergence.

An analytical formulation of the equations of motion of this model was developed, including unsteady aerodynamic loads in an s-plane or

time domain form. The result was a state-space representation of the equations of motion. The structural design variable was taken to be the shear center position with respect to the airfoil midchord, denoted as a_e in Figure 1. This parameter is nondimensional with respect to the airfoil semi-chord dimension, b, and is taken to be positive if the shear center lies aft of the airfoil midchord. As a result, the limits to a_e are $-1 < a_e < 1$.

Optimal steady-state linear quadratic regulator theory (SSLQR) was used to synthesize full-state feedback control laws to stabilize the model at different airspeeds (represented in nondimensional form as $\overline{U}_{DES}$) and different values of a_e. Figure 2 shows the "open-loop", control-off, stability boundaries for the model dimensions chosen, but with a_e taken to be a design parameter capable of being chosen arbitrarily. In Figure 2, the parameter b_{CT}/b represents the ratio of tail surface area to wing surface area. Note that full body pitch restraint or "clamping" the fuselage reduces the flutter and divergence boundaries to those of the 3-degree-of-freedom airfoil alone. The use of SSLQR theory to synthesize control laws with the shear center at various positions uses a measure of state and control activity at a fixed design airspeed, $\overline{U}_{DES}$, as a cost function, J, to be minimized. Values of this function J for this idealization are plotted versus a_e and design airspeed, $\overline{U}_{DES}$, in Figure 3. While the absolute value of J has no physical significance, the relatively large values of J near $a_e = -0.4$ and $\overline{U}_{DES} = 6$ indicate that the active control is experiencing difficulty stabilizing the system in this region.

These regions of relatively high cost correspond to configurations for which the system experiences near-uncontrollability of unstable

modes. This is indicated in Figure 4 by the close proximity of zeros of
the loop transfer matrix to some system poles (eigenvalues) near the $j\omega$
axis.

A similar contour plot for control cost was constructed for the
airfoil model with rigid body pitch freedom suppressed. This contour
plot, shown in Figure 5, indicates that high cost regions are also
present, particularly where open-loop divergence is to be stabilized.
It would appear that a design procedure that can select low control cost
regions at a fixed design airspeed would be sufficient to the integrated
optimal design task. Such is not the case, as indicated in Figure 6.

Figure 6 shows the closed-loop stability boundaries of the actively
controlled 3-degree-of-freedom airfoil model, as functions of shear
center position, a_e. Open-loop stability boundaries are superimposed on
this figure. Figure 6 was constructed by choosing a large number of a_e
values and then constructing a control law with $\overline{U}_{DES}$ held fixed at 6.0.
Thus, while $\overline{U}_{DES}$ held fixed at 6.0, the control law changes with a_e in
Figure 6. The high control cost region near $a_e = -0.4$ also includes
instabilities below the design speed. Thus, while the active control
has extended the upper part of the flight envelope, in this region a new
instability associated with off-design airspeeds has appeared. For this
reason, the cost function from SSLQR theory is inadequate as a sole per-
formance index to be used in the integrated design process. To remedy
this, a combined design procedure based upon multi-level linear decompo-
sition [1] of the aeroservoelastic system into structural and control
subsystems was formulated. For this procedure, the overall design
objective was maximization of the stable airspeed envelope with a struc-
tural parameter (a_e) and control parameters from SSLQR theory as design

variables.

With multi-level, linear decomposition, the subsystem designs are themselves in some measure optimal. Optimal sensitivity derivatives are computed with respect to specified system parameters to aid in choosing a new design that is both optimal on the subsystem level, yet satisfies the global objectives at the system level. In this case, analytical expressions for the changes in the eigenvalues of the closed-loop system (subject to the constraint that the system is optimally controlled) were constructed using a method proposed by Gilbert [2]. No structural cost was associated with changes in the shear center position, representing a limiting case such as might be present in a laminated wing structure. This assumption does not, however, limit the future applications of the procedure. To assess system stability, a stability index F_{sj} is defined such that

$$F_{sj} = \frac{1}{\rho} \ln \left(\sum_{i=1}^{N} e^{\rho \sigma_i} \right)$$

where ρ is a weighting function (in this case, $\rho = 1$), N is equal to the number of potentially critical eigenvalues, σ_i is the real part of the ith eigenvalue and $\overline{U}_j$ is the airspeed at which F_{sj} is computed ($\overline{U}_j \neq \overline{U}_{DES}$). If $F_{sj} < 0$ then the system is stable. If $F_{sj} > 0$ then the system is to be stabilized by finding the proper combination of a_e and control parameters that will minimize F_{sj}.

The design procedure begins with the choice of initial values of a_e and other system parameters. Next, a control law is synthesized at $\overline{U}_{DES}$. An airspeed $\overline{U}_k$ is chosen for which the closed-loop system is unstable ($F_{sk} > 0$). The derivatives of F_{sk} with respect to a_e and $\overline{U}_{DES}$ are computed, subject to the constraint that the active control law is

optimal. In addition, derivatives of other stability indices at lower airspeeds, $\bar{U}_j$, $(\bar{U}_j < \bar{U}_k)$, with respect to these variables are also computed. An optimization procedure based upon a simplex algorithm uses this sensitivity information to choose changes in a_e and $\bar{U}_{DES}$ to minimize F_{sk}, without allowing other F_{sj} values to become positive (unstable).

If the value of F_{sk} is found to be negative on a certain design cycle (the system is thus stable at $\bar{U}_k$), the airspeed $\bar{U}_k$ becomes a subcritical airspeed. A new, post-critical airspeed is then chosen as $\bar{U}_k$ and the procedure continues. The procedure terminates when $\bar{U}_k$ is either equal to the desired maximum stable airspeed or when no further stabilization is possible. Figure 7 illustrates this procedure.

For this example, the nondimensional airspeeds $\bar{U}_j$ at which stability was required were chosen (arbitrarily) to be integers, thus $\bar{U}_j = j$ in Figure 7. Initially, the system is unstable at $\bar{U}_k = 7.0$ with a <u>control</u> design airspeed of $\bar{U}_{DES} = 6.0$. The first design iteration reduces the measure of instability F_{sk} by instructing the "structures group" to shift the shear center aft towards the mid-chord and asking the "controls group" to reduce the value of its design airspeed. At design cycle 4 the actively controlled system is stable at $\bar{U}_7 = 7.0$ so it is now required that the closed-loop system attempt stabilization at $\bar{U}_k = 8.0$. This task is achieved at design cycle 7. At this point, the requirement is changed to attempt closed-loop stability at $\bar{U}_k = 9.0$. Figure 7(b) indicates that this objective cannot be met; however, F_{sk}, at $\bar{U}_k = 9$ is minimized. The root locus plot (using airspeed as the gain) of the final, actively controlled system is shown in Figure 8.

Figure 8 shows that the final design is a compromise between flutter in two different modes. The paper discusses the reasons for arriving at this result. It is interesting to note that the optimal actively controlled structural configuration does not correspond to the structural configuration that one would find if only passive tailoring were used to increase stability.

The SSLQR theory requires the user to choose weighting matrices in the cost function J. These elements are found to have a significant effect, in some cases, upon the appearance of sub-critical stability regions. As a result, a second example was chosen to illustrate the use of a state weighting element Q_θ, (the weighting on rigid body pitch), as a design parameter. In addition, the position of the airfoil with respect to the pivot, given as the dimension $b\bar{x}$ in Figure 1 was also treated as a design parameter, together with $\bar{U}_{DES}$ and a_e.

Figure 9 shows the design cycle history for the 4-degree-of-freedom wing configuration, which includes rigid-body pitch. The initial objective was to stabilize the system at $\bar{U}$ = 4.0 and 5.0 using Q_θ and $\bar{U}_{DES}$ as design variables. Note that the closed-loop system is stable at $\bar{U}$ = 6.0. By design cycle number 7, the procedure was experiencing difficulty meeting its objectives. At this point, the position of the wing, with respect to the pivot, $b\bar{x}$, was allowed to change, together with a_e, for the next two iterations. After cycle 9, a_e and $\bar{x}$ were held fixed and optimization continued using $\bar{U}_{DES}$ and Q_θ as design variables.

The effects of the use of $b\bar{x}$ and a_e as parameters can be seen in Figure 10. Figure 10 plots the partial derivatives of the stability indices, with respect to Q_θ, as functions of design cycle number. This figure indicates that changes in $b\bar{x}$ and a_e increase the magnitudes of

these derivatives. As a result, Q_θ becomes more effective as a design parameter.

Figure 11 shows the root-locus plots, with $\overline{U}$ as a gain, for the initial closed-loop design and the final closed-loop design. The final design is seen to be a compromise between flutter at $\overline{U}$ = 7.04 and flutter in a hump mode at around $\overline{U}$ = 5.0. If one were to try to further increase the $\overline{U}$ = 7.04 flutter speed, the stability constraint at $\overline{U}$ = 5.0 would be violated.

The paper will describe additional features of this integrated design technique. Included will be additional data indicating why several of the features observed in the previous figures occur as they do. In addition, a discussion will be included as to how this procedure may be expanded to include control synthesis by techniques other than SSLQR theory.

References

1. Sobieszczanski-Sobieski, J., James, B., and Dovi, A., "Structural Optimization by Multilevel Decomposition," AIAA/ASME/ASCE/AHS 24th Structures, Structural Dynamics and Materials Conference Proceedings, AIAA paper no. 83-0832-CP, May 2-4, 1983.

2. Gilbert, M.G., "Optimal Linear Control Law Design Using Optimum Parameter Sensitivity Analysis," Proposal for Doctoral Dissertation Research, Purdue University, School of Aeronautics and Astronautics, 1983.
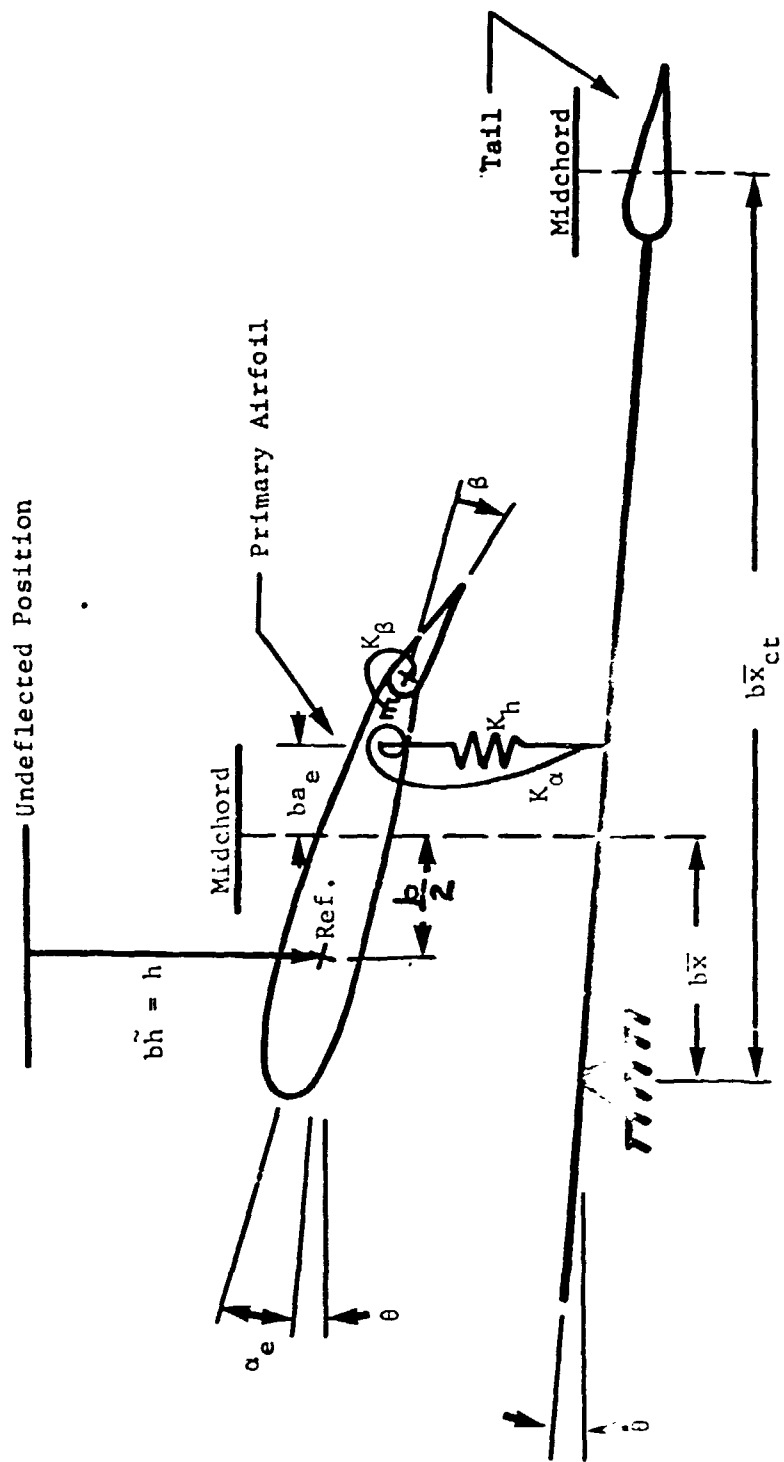
Figure 1 — 4-degree-of-freedom aeroelastic model showing geometrical parameters and degrees of freedom α_e, θ, β and h.
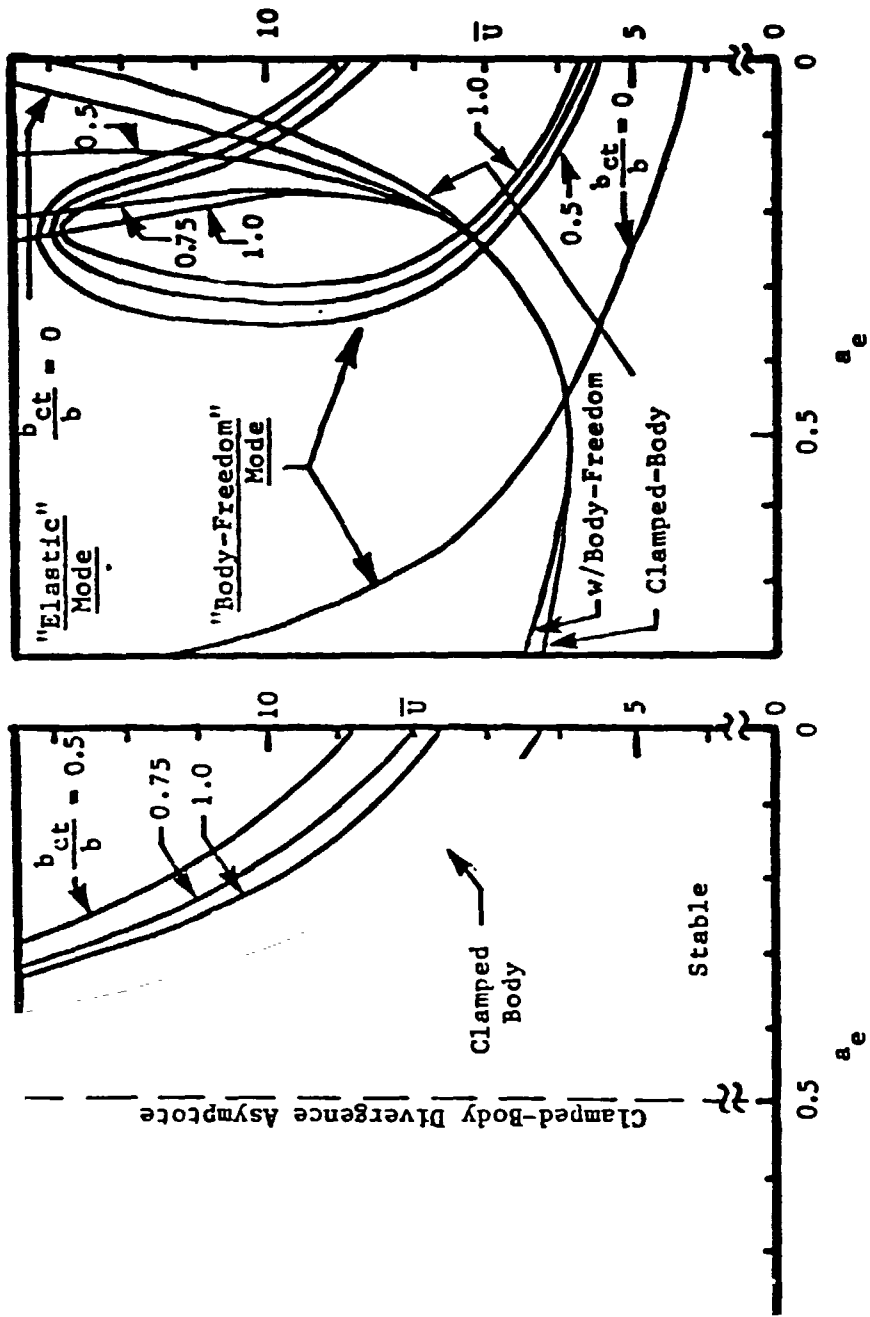
Figure 2 – The effect of 4-degree-of-freedom model shear center position a_e upon open loop stability boundaries with the ratio of tail surface area-to-airfoil surface area $(\frac{b_{ct}}{b})$ as a parameter; $\bar{x} = 5$, $x_{ct} = 10$.
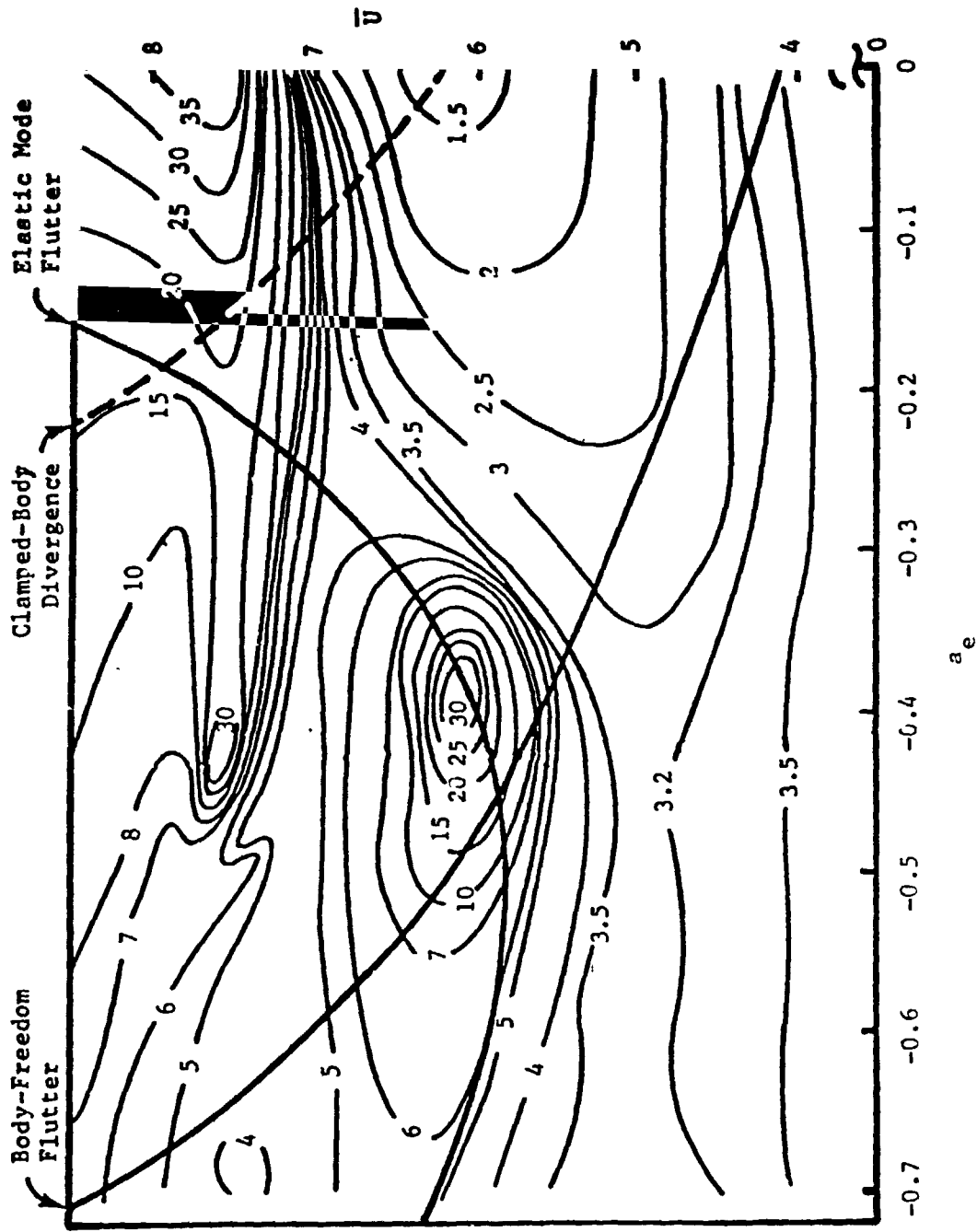
a. Divergence

b. Flutter

Figure 3 – 4-degree-of-freedom aeroelastic model minimum control cost contours as a function of shear center position, a_e, and control design speed, $\bar{U}_{DES}$; no tail surface, stable wing/fuselage combination. Open loop stability boundaries are overlaid.
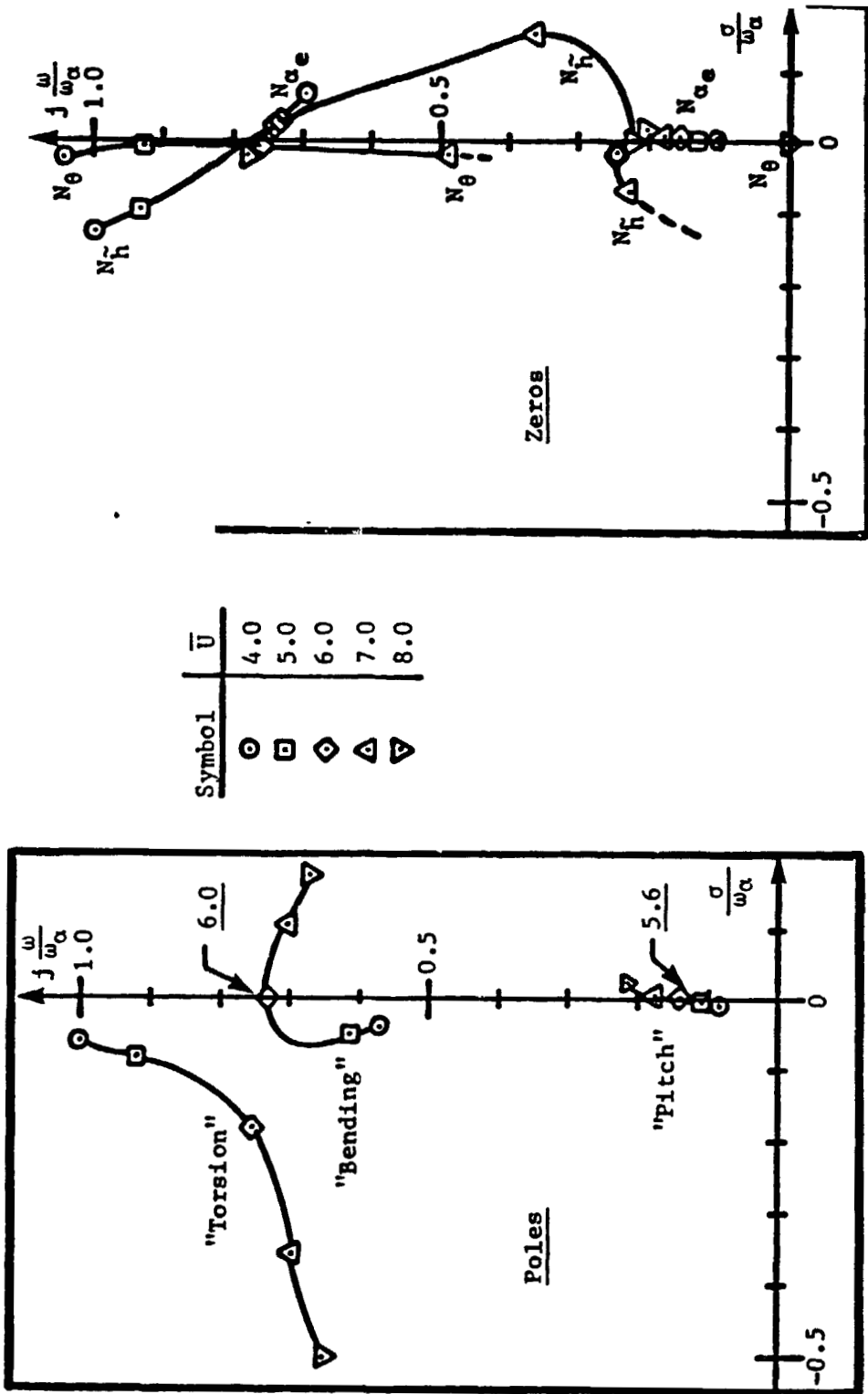
Figure 4 – System poles and loop transfer matrix zeroes for the 4-dof model with $a_e = -0.4$, $\frac{\tilde{x}}{\tilde{x}} = 5$ and no tail.
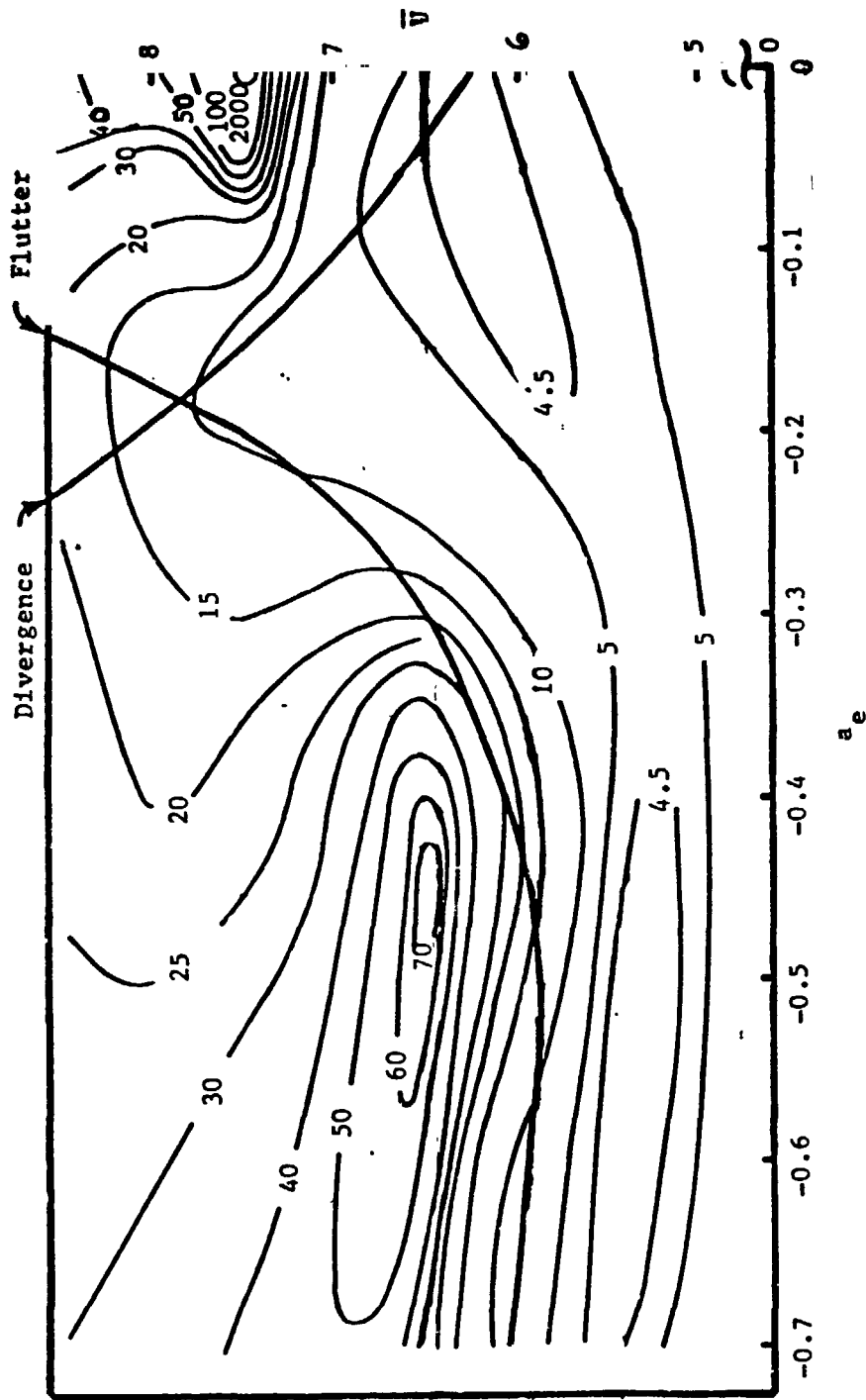
Figure 5 – Rigid-body pitch restrained, 3-dof aeroelastic model, minimum control cost contours as a function of shear center position, a_e, and control design speed $\overline{U}_{DES}$. Open-loop stability boundaries are overlaid.
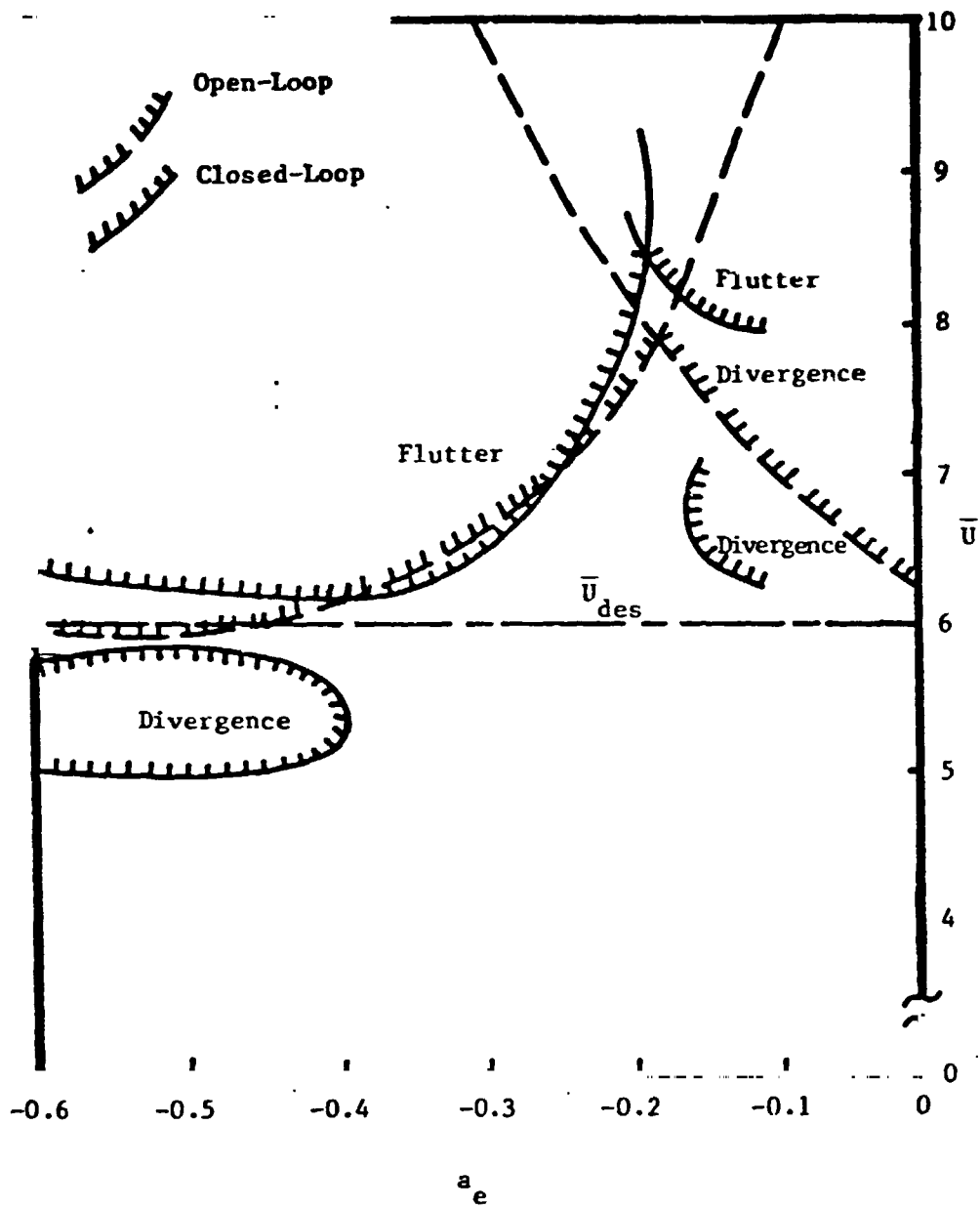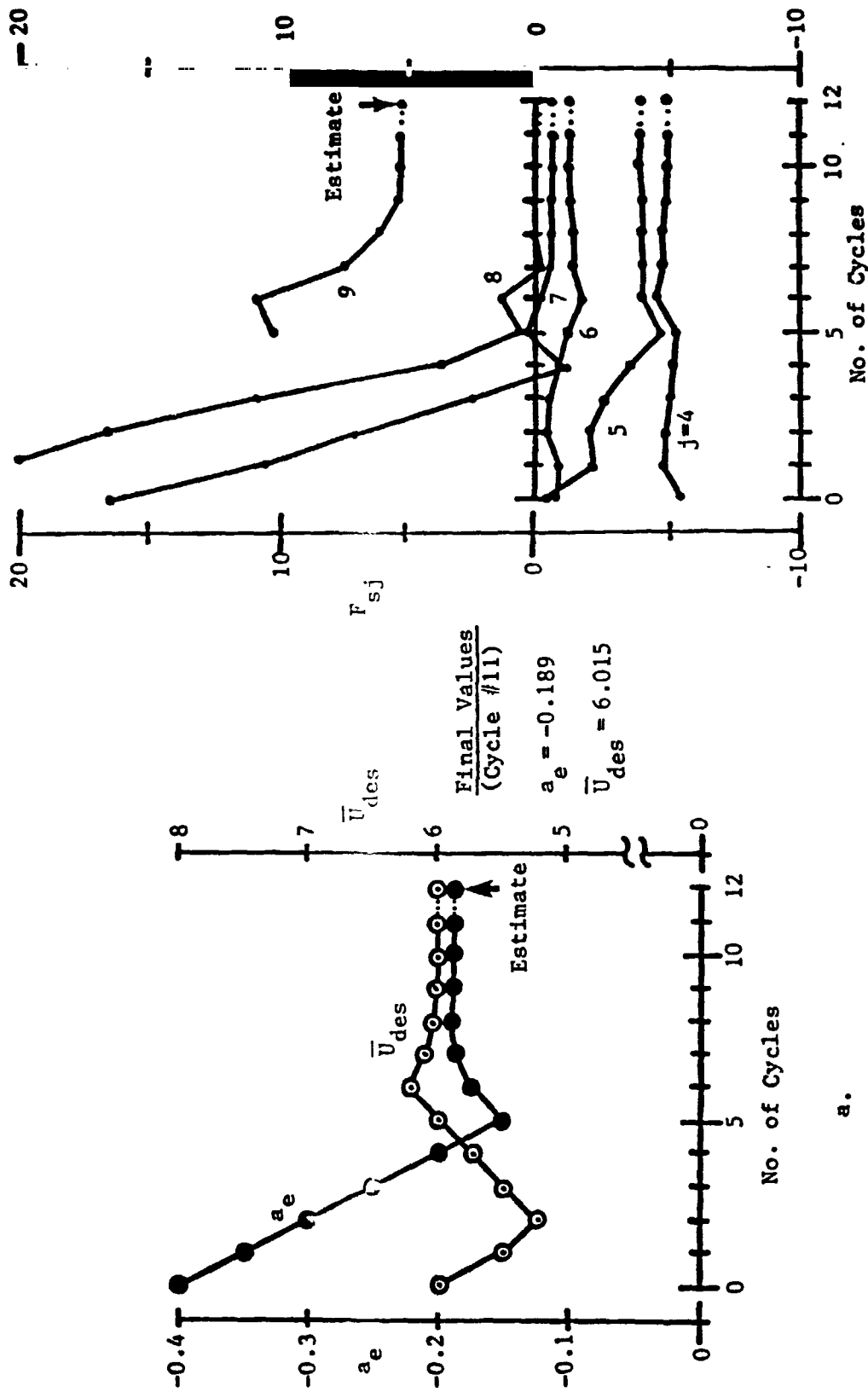
Figure 6 - Open and closed-loop stability boundaries as a
function of a_e for the 3-dof aeroelastic
model; control laws are synthesized at $\overline{U}_{DES} = 6.0$

Figure 7 — Design cycle histories using a_e and $\overline{U}_{DES}$ as design parameters; (a) a_e and $\overline{U}_{DES}$ as a function of design cycle number; (b) the stability indices as functions of design cycle number.
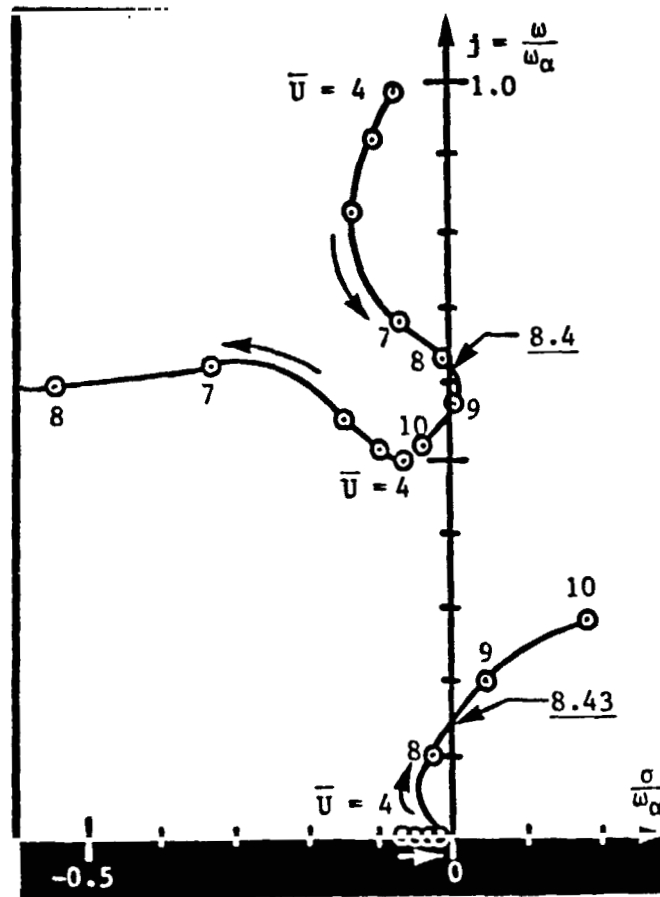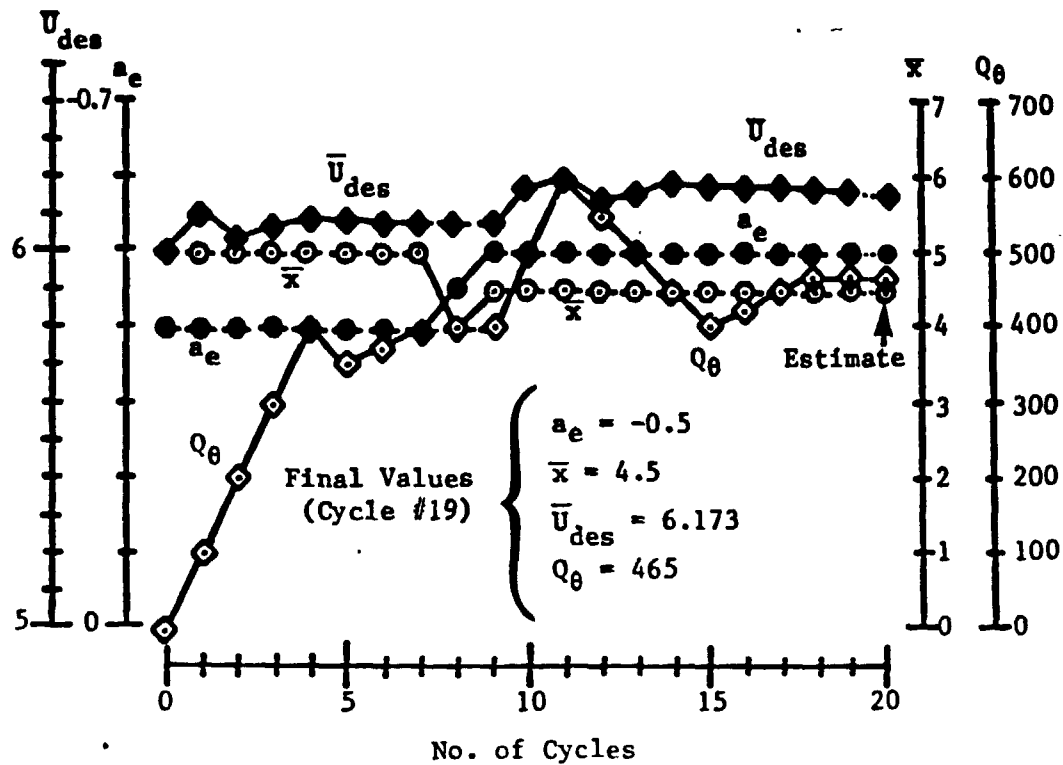
15

Figure 8 - Velocity root loci, design cycle #11 for the
3-dof aeroelastic model.

a. Design Parameters
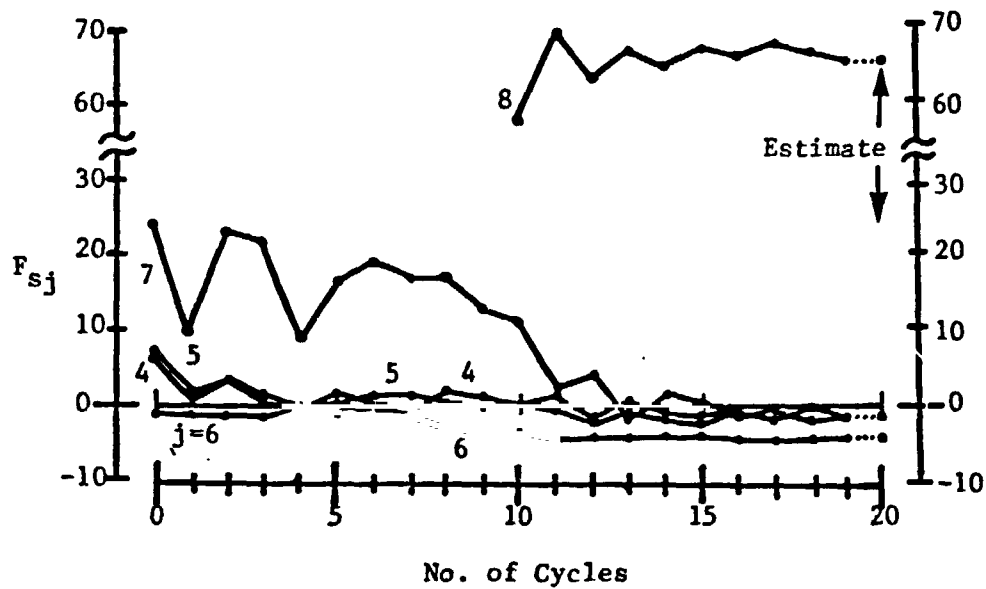
b. Stability Indices

Figure 9 - Design cycle histories for the 4-dof aeroelastic
model example.
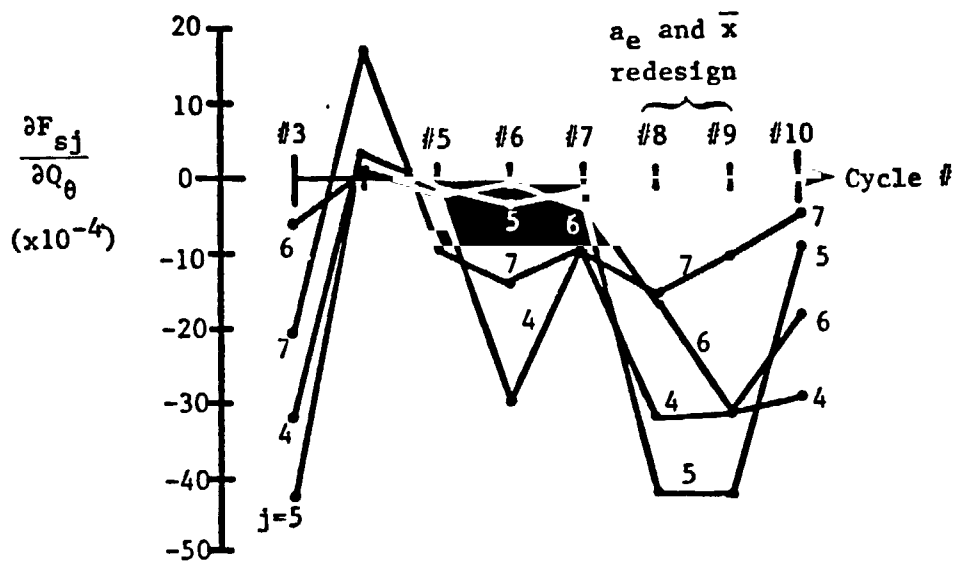
Figure 10- The value of $\partial F_{sj}/\partial \theta_\theta$ as a function of design cycle number for the 4-dof aeroelastic model.
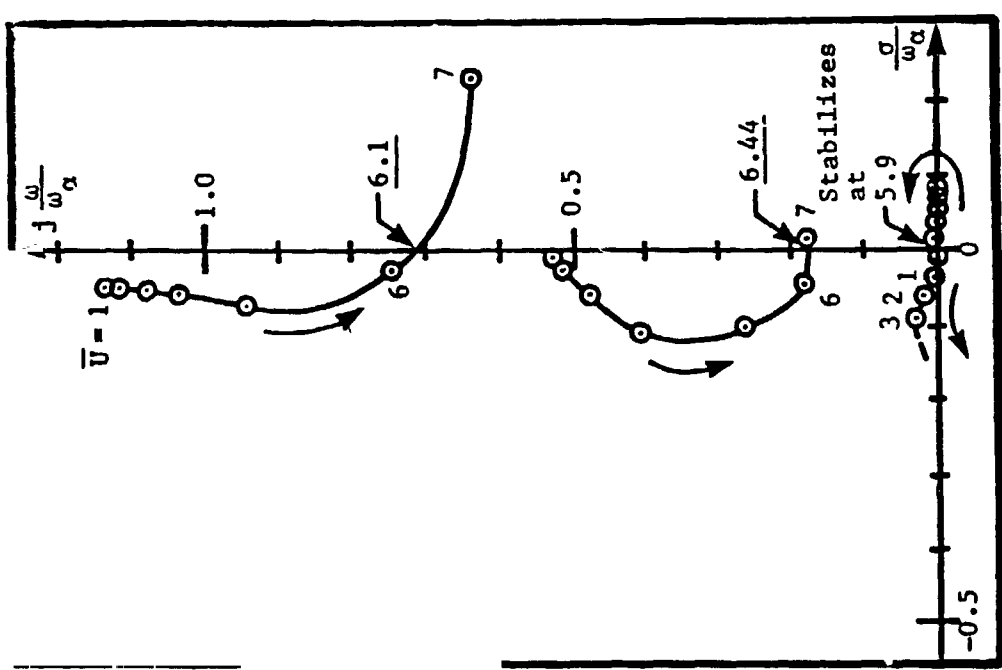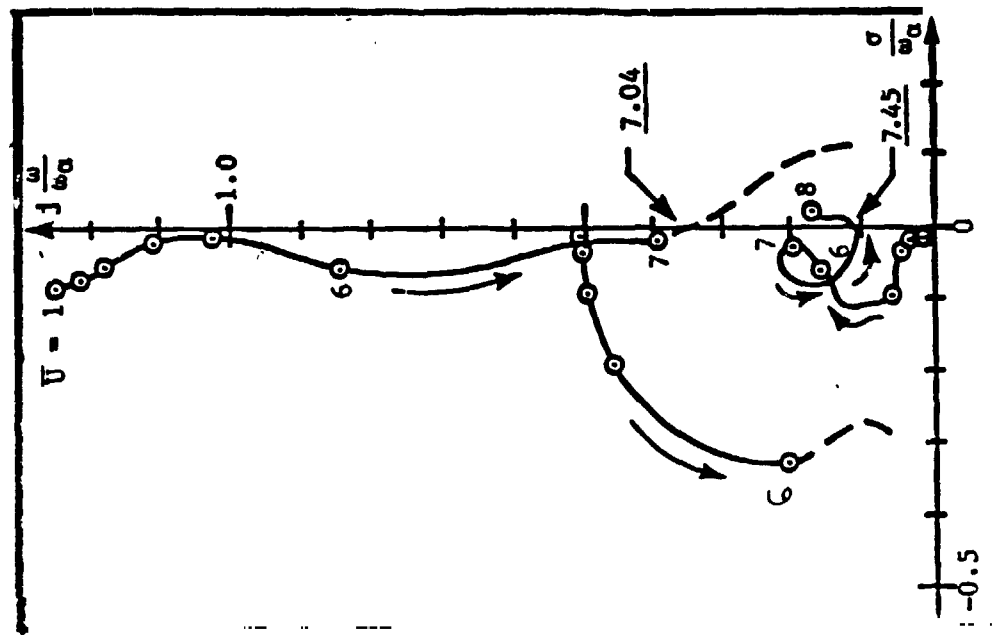
Figure 11– Velocity root locus diagrams for: (a) the initial design; (b) the final design of the 4-dof aeroelastic model.

APPENDIX B

The attached document summarizes the development of a two-degree
of freedom idealization used to study the interaction between
directional stiffness and feedback control. This model was developed
by Professor Weisshaar and has been implemented on the computer by
Mr. Sallee. A two-mode flexible model could also be used. However,
past experience with the semi-rigid model has been quite good. As a
result, it is the choice for demonstration purposes.

An Idealized Aeroelastic Model for Active Control Studies

Consider the idealized lifting surface shown in Figures 1, 2, 3. The surface itself is rigid, but is attached to a pivot on a wall; it has mass uniformly distributed along the span. A reference axis, the y-axis in Figure 2, is used for the determination of the equations of motion; the reference axis lies a distance ba aft of the midchord. The line of aerodynamic centers is located at a distance ba_c ahead of the airfoil midchord and is shown in Figure 3. For the position shown, $b(a-a_c)$ is a negative quantity. The chordwise offset of the line of centers of mass from the reference axis is denoted as x_α; this latter coordinate is positive when the sectional centers of mass are located aft of the reference axis.

The downward deflection of the line of centers of mass is denoted as z. This deflection and the velocity $\dot{z}$ are expressed in terms of the torsional rotation, θ, and "bending" rotation, ϕ, as:

$$z = x_\alpha \theta - \phi y \tag{1}$$

$$\frac{dz}{dt} = \dot{z} = x_\alpha \dot{\theta} - \dot{\phi} y \tag{2}$$

The airfoil has constant mass per unit length, m, so that the kinetic energy, T, may be written as:

$$T = \frac{1}{2} \{I_0 \dot{\theta}^2\} 1 + \frac{1}{2} \int_0^\ell m \dot{z}^2 dy \tag{3}$$

or

$$T = \frac{1}{2} \{I_0 + m x_\alpha^2\} \ell \dot{\theta}^2 - m x_\alpha \ell^2 \ddot{\theta}\phi + m \frac{\ell^3}{3} \dot{\phi}^2 \tag{4}$$

where I_0 is the pitch mass moment of inertia per unit length of each section along the wing surface, taken about the line of centers of mass. The strain energy in the spring supports due to deformations θ and ϕ is:
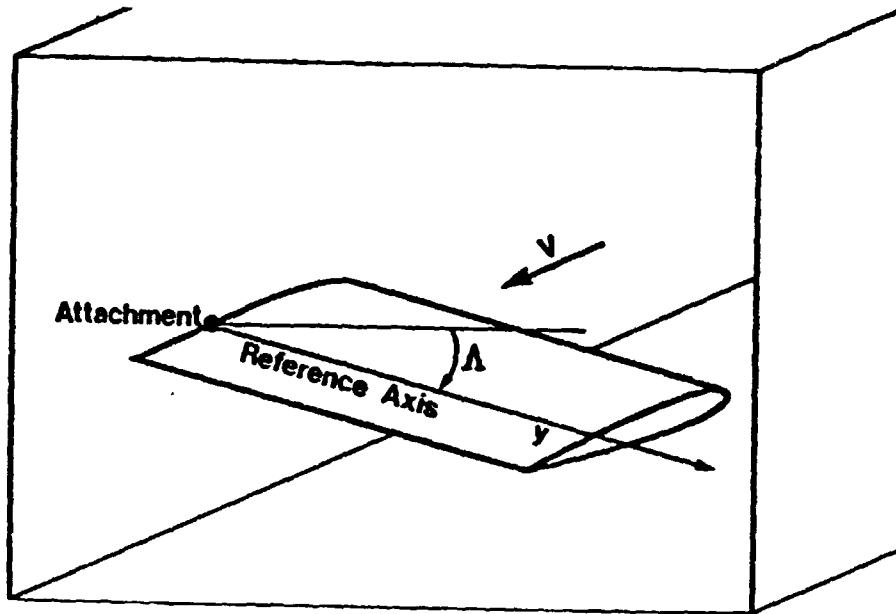
Figure 1 - Idealized airfoil, shown swept at an angle Λ to the airstream
and attached to a pivot on the wind-tunnel wall.
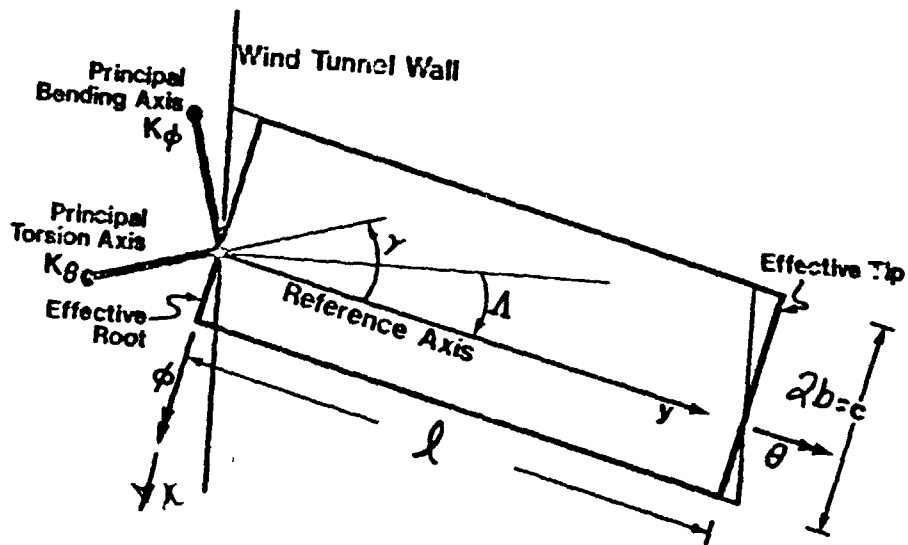
Figure 2 - Planform view of 2-D, idealized airfoil showing: rotational
deformations θ and ϕ; orientation of principal bending and
torsion axes, ∂; and, effective root and tip approximations.
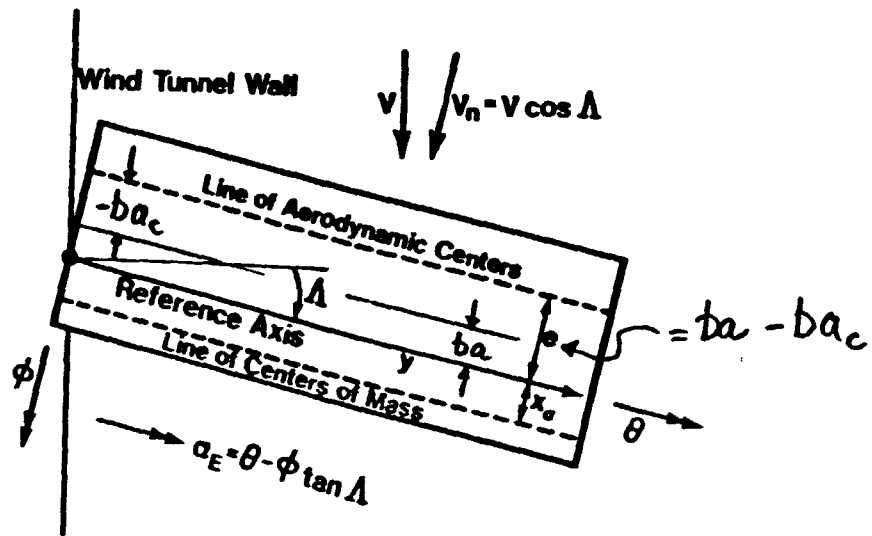
Figure 3 – Planform view of idealized airfoil showing: aerodynamic
center/reference axis offset; reference axis/center of
mass offset; reference axis/milchord offset distance, ba;
and, normal component of velocity, V_n.

Figure 4 - Full span control surface model.

$$U = \frac{1}{2} K_\theta \{\theta \cos \gamma - \phi \sin \gamma\}^2 \tag{5}$$
$$+ \frac{1}{2} K_\phi \{\phi \cos \gamma + \theta \sin \gamma\}^2$$

From Lagrange's equations the equations of motion for free vibration in the absence of airloads are found to be:

$$\begin{vmatrix} \ell(I_0 + mx_\alpha^2) & -\frac{m}{2}x_\alpha\ell^2 \\ -\frac{m}{2}x_\alpha\ell^2 & \frac{m\ell^3}{3} \end{vmatrix} \begin{vmatrix} \ddot{\theta} \\ \ddot{\phi} \end{vmatrix} + \begin{vmatrix} K_\theta\cos^2\gamma + K_\phi\sin^2\gamma & (K_\phi - K_\theta)\cos\gamma\sin\gamma \\ (K_\phi - K_\theta)\sin\gamma\cos\gamma & K_\theta\sin^2\gamma + K_\phi\cos^2\gamma \end{vmatrix} \begin{vmatrix} \theta \\ \phi \end{vmatrix} = \begin{vmatrix} 0 \\ 0 \end{vmatrix} \tag{6}$$
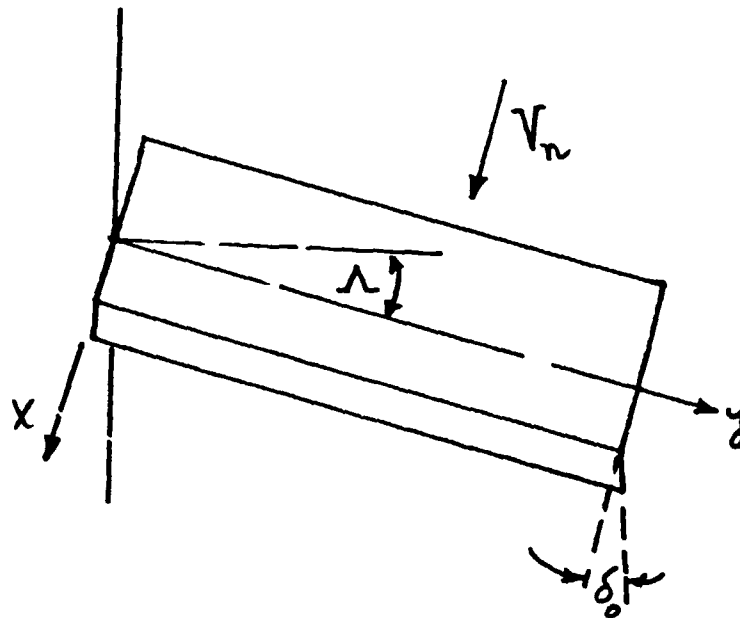
To simplify the writing of these equations, elements of the matrices in Eqn. 6 are defined as follows.

Inertia terms

$$m_{11} = m\ell\{x_\alpha^2 + r_0^2\} = m\ell r_\alpha^2 \quad \text{where } r_0^2 = \frac{I_0}{m}$$
$$m_{12} = -m\ell\{\frac{x_\alpha \ell}{2}\}$$
$$m_{22} = m\ell\{\frac{\ell^2}{3}\}$$

(Note that $m\ell$ is the total mass of the idealized wing.)

Stiffness terms

$$k_{11} = K_\theta\cos^2\gamma + K_\phi\sin^2\gamma$$
$$k_{12} = (K_\phi - K_\theta)\cos\gamma \sin\gamma$$
$$k_{22} = K_\theta\sin^2\gamma + K_\phi\cos^2\gamma$$

Aerodynamic Forces

Aerodynamic forces due to the motion of the idealized airfoil, can be related to the two degrees of freedom, θ and ϕ. For the present analysis these forces were computed from modified aerodynamic strip theory as outlined by Yates in Reference 1. The pitching moment about the y-axis in Figure 3 is denoted as M_θ, while bending moment about the

x-axis, located at the root, is M_ϕ.

The aerodynamic load per unit length along the swept y-axis is P. The load P is positive when it acts in the upward direction, out of the plane of the paper. In the present case, this load is [1]:

$$P = \pi\rho b^2 [-\ddot{\phi} y + V_n \dot{\theta} - V_n \dot{\phi}\tan\Lambda - ba\ddot{\theta}]$$
$$+ c_{1_\alpha} \rho V_n bC(k)Q \tag{7}$$

where Q is the downwash velocity at the control point on the airfoil. The Theodorsen function $C(k)$ is valid only when ϕ and θ are simple harmonic functions of time. The downwash is:

$$Q = -\dot{\phi}y + V_n(\theta-\phi\tan\Lambda) + b(\frac{c_{1_\alpha}}{2\pi} + a_c -a)\dot{\theta} \tag{8}$$

In Eqn. 8, the term a_c represents the distance, measured in semi-chords, that the static aerodynamic center lies behind the wing mid-chord position. For subsonic flow this term is negative. For incompressible flow conditions, $a_c = -\frac{1}{2}$, since the aerodynamic center will be at the airfoil quarter-chord position.

The aerodynamic pitching moment, per unit length, measured positive nose-up about the reference axis is:

$$M_\alpha = -\pi\rho b^4(\frac{1}{8}+a^2)\ddot{\theta} - \pi\rho b^2 V_n(\dot{\phi}y+V_n\phi\tan\Lambda)$$
$$- \pi\rho b^3 a(\ddot{\phi}y+V_n\dot{\phi}\tan\Lambda) + \pi\rho b^2 V_n^2\theta$$
$$- 2\pi\rho V_n b^2[\frac{1}{2} - (a-a_c)C(k)\frac{c_{1_\alpha}}{2\pi}]Q \tag{9}$$

To develop the equations for the motion dependent airloads, we define the moments M_θ and M_ϕ as follows

$$M_\theta = \int_o^\ell M_\alpha dy \tag{10}$$

$$M_\phi = \int_o^l Pydy \tag{11}$$

Equations 10 and 11 can be written as

$$\begin{Bmatrix} M_\theta \\ M_\phi \end{Bmatrix} = mlr_\alpha^2\omega_p^2 \begin{Bmatrix} \overline{M}_\theta \\ \overline{M}_\phi \end{Bmatrix} \tag{12}$$

In Eqn. 12, ω_p is a reference frequency. When motion of the form

$$\begin{Bmatrix} \theta \\ \phi \end{Bmatrix} = \begin{Bmatrix} \overline{\theta} \\ \overline{\phi} \end{Bmatrix} e^{st} \tag{13}$$

is assumed, expressions for $\overline{M}_\theta$ and $\overline{M}_\phi$ can be constructed. These expressions are written symbolically as follows:

$$-\begin{Bmatrix} \overline{M}_\theta \\ \overline{M}_\phi \end{Bmatrix} = \left| (\frac{s}{\omega_p})^2 [M_{ij}] + (\frac{s}{\omega_p})[Bij] + [A_{ij}] \right| \begin{Bmatrix} \overline{\theta} \\ \overline{\phi} \end{Bmatrix} \tag{14}$$

Elements of the $[M_{ij}]$ matrix are the apparent mass terms for this airfoil, while the $[B_{ij}]$ matrix represents the aerodynamic damping. $[A_{ij}]$ is the aerodynamic stiffness matrix. The elements of these three matrices may be conveniently defined in terms of a group of parameters. These parameters are:

$$\overline{V}_n = V\cos\Lambda/b\omega_p \tag{15}$$

$$C_L = 2\pi(\frac{1}{2} -(a-a_c)C(k)C_{l_\alpha}/2\pi) \tag{16}$$

$$C_p = a_c - a + C_{l\alpha}/2\pi \tag{17}$$

$$\overline{r}_\alpha = r_\alpha/b \tag{18}$$

$$\mu = m/\pi\rho b^2$$

$$d = \mu\overline{r}_\alpha^2 \tag{19}$$

(AR) = structural aspect ratio = $1/2b$

The matrix elements are then written as follows:

$$M_{11} = (\tfrac{1}{8} + a^2)/d \tag{20}$$

$$M_{12} = M_{21} = a(AR)/d \tag{21}$$

$$M_{22} = \frac{4(AR)^2}{3d} \tag{22}$$

$$B_{11} = \frac{C_L C_p \overline{V}_n}{\pi d} \tag{23}$$

$$B_{12} = ((AR) + a \tan\Lambda - \frac{C_L(AR)}{\pi})(\frac{\overline{V}_n}{d}) \tag{24}$$

$$B_{21} = (-(AR) - \frac{c_{1_\alpha}}{\pi} C_p(AR)C(k)) \frac{\overline{V}_n}{d} \tag{25}$$

$$B_{22} = (AR)(\tan\Lambda + \frac{4}{3} \frac{c_{1_\alpha}}{\pi} (AR)C(k))\frac{\overline{V}_n}{d} \tag{26}$$

$$A_{11} = \frac{\overline{V}_n^2}{d} (-1 + \frac{C_L}{\pi}) \tag{27}$$

$$A_{12} = \frac{\overline{V}_n^2}{d} (\tan\Lambda - \frac{C_L \tan\Lambda}{\pi}) \tag{28}$$

$$A_{21} = \frac{\overline{V}_n^2}{\pi d} (-c_{1_\alpha} (AR)C(k)) \tag{29}$$

$$A_{22} = \frac{\overline{V}_n^2}{\pi d} (c_{1_\alpha} (AR)C(k)\tan\Lambda) \tag{30}$$

The equations of motion are written as

$$[s^2[m_{ij}] + [k_{ij}]]\begin{Bmatrix} \overline{\theta} \\ \overline{\phi} \end{Bmatrix} + m l r_\alpha^2 \omega_p^2 \begin{Bmatrix} \overline{M}_\theta \\ \overline{M}_\phi \end{Bmatrix} = 0 \tag{31}$$

Dividing by the factor $m l r_\alpha^2 \omega_p^2$ gives the following equations:

$$\begin{bmatrix} (\overline{s}^2 + 1) & (\overline{s}^2[\dfrac{-\overline{x}_\alpha(AR)}{\overline{r}_\alpha^2}] - \dfrac{\psi}{\backslash|\overline{R}}) \\[4mm] (\overline{s}^2[\dfrac{-\overline{x}_\alpha(AR)}{\overline{r}_\alpha^2}] - \dfrac{\psi}{\backslash|\overline{R}}) & (\overline{s}^2[\dfrac{4(AR)^2}{3\overline{r}_\alpha^2}] + \dfrac{1}{R}) \end{bmatrix} \begin{Bmatrix} \overline{\theta} \\ \overline{\phi} \end{Bmatrix} \tag{32}$$

$$+ \, [\bar{s}^2[M_{ij}] + \bar{s}[B_{ij}] + [A_{ij}]] \; \begin{array}{c} \bar{\theta} \\ \overline{} \\ \bar{\phi} \end{array} = \begin{array}{c} 0 \\ \\ 0 \end{array} \qquad (32) \; \text{concluded}$$

The parameter $\bar{x}_\alpha$

$$\bar{x}_\alpha = x_\alpha / b \qquad (33)$$

while

$$\psi = -K_{12} / \sqrt{\overline{K_{11} K_{22}}} \qquad (34)$$

and

$$R = K_{11} / K_{22} \qquad (35)$$

These matrix equations may be combined and written as

$$[\bar{s}^2[M_T] + \bar{s}[B] + [K_T]] \left\{ \begin{array}{c} \bar{\theta} \\ \overline{} \\ \bar{\phi} \end{array} \right\} = \left\{ \begin{array}{c} 0 \\ 0 \end{array} \right\} \qquad (36)$$

where

$$[M_T] = [m_{ij}] + [M_{ij}] \qquad (37)$$

$$[K_T] = [k_{ij}] + [A_{ij}] \qquad (38)$$

This equation may also be written as follows:

$$[M_T]\{\ddot{x}\} = -[B]\{\dot{x}\} - [K_T]\{x\} \qquad (39)$$

where $\{x\} = \left\{ \begin{array}{c} \bar{\theta} \\ \overline{} \\ \bar{\phi} \end{array} \right\}$ and $(\dot{}) = \dfrac{d()}{d(\omega_p t)}$. This, in turn can be used to recast

the problem in the following form:

$$\left\{ \begin{array}{c} \dot{x} \\ \ddot{x} \end{array} \right\} = \left| \begin{array}{cc} 0 & I \\ -M_T^{-1} K_T & -M_T^{-1} B \end{array} \right| \left\{ \begin{array}{c} x \\ \dot{x} \end{array} \right\} \qquad (40)$$

If the vector $\{\eta\}$ is defined as

$$\{\eta\} = \left\{ \begin{array}{c} x \\ \dot{x} \end{array} \right\} \qquad (41)$$

where {η} represents a vector of system states, then

$$\{\dot{\eta}\} = [A]\{\eta\} \qquad (42)$$

The eigenvalues of [A] determine the natural frequencies and damping in the system.

Eigenvalue Sensitivity Derivatives

The objective of this section is to outline a procedure for calculating the first-order changes (first derivatives) in system eigenvalues due to changes in system parameters ψ, R and $\overline{V}$. these derivatives will be used to estimate the effects upon stability of a change in stiffness cross-coupling (ψ), primary stiffness ratio (R) or airspeed ($\overline{V}$).

Begin by defining the eigenvalue problem at a given airspeed $\overline{V}$.

$$\overline{s}\{\eta\} = [A]\{\eta\} \qquad (42)$$

The solution to Eqn. 42 is written as:

$$\lambda_i\{e_i\} = [A_{ij}]\{e_i\} \qquad (43)$$

where λ_i is an eigenvalue corresponding to the eigenvector $\{e_i\}$. The eigenvalue λ_i and the vector $\{e_i\}$ may be complex.

The parameters ψ, R and $\overline{V}$ may be represented, in general, by the symbol p. Let's differentiate Eqn. 43 with respect to p.

$$\frac{\partial\lambda_i}{\partial p}\{e_i\} + \lambda_i\{\frac{\partial e_i}{\partial p}\} = \left|\frac{\partial A_{ij}}{\partial p}\right|\{e_i\} + [A_{ij}]\{\frac{\partial e_i}{\partial p}\} \qquad (44)$$

Equation 44 now may be written as:

$$\frac{\partial\lambda_i}{\partial p}\{e_i\} = \left|\frac{\partial A_{ij}}{\partial p}\right|\{e_i\} + \left|[A_{ij}] - \lambda_i[I]\right|\{\frac{\partial e_i}{\partial p}\} \qquad (45)$$

We are only interested in the change in λ_i, not the change in the eigenvector e_i. To eliminate $\partial e_i/\partial p$ from Eqn. 45, consider the so-called "left-hand" or transpose eigenvalue problem defined as:

$$[A_{ij}]^T\{r_i\} = \lambda_i\{r_i\} \qquad (46)$$

Equation 46 defines an eigenvalue problem for the matrix transpose of $[A_{ij}]$. The eigenvalues of Eqn. 46 will be the same as those found in

Eqn. 43, since the determinant of the matrix transpose is the same as the determinant of the matrix. As a result, both Eqns. 43 and 46 have the same characteristic equations. However, the eigenvectors $\{r_i\}$ and $\{e_i\}$ associated with λ_i are _not_ identical unless $[A] = [A]^T$, that is, unless the $[A]$ matrix is symmetrical. Equation 46 is important; taking its matrix transpose, it becomes:

$$\{r_i\}^T \left| [A] - \lambda_i[I] \right| = 0 \tag{47}$$

Notice the similarity between the term in Eqn. 47 and the last term in Eqn. 45. Pre-multiplying Eqn. 45 by $\{r_i\}^T$, we get

$$\frac{\partial \lambda_i}{\partial p} \lfloor r_i \rfloor \{e_i\} = \lfloor r_i \rfloor \left| \frac{\partial A_{ij}}{\partial p} \right| \{e_i\} \tag{48}$$
$$+ \lfloor r_i \rfloor \left| [A] - \lambda_i[I] \right| \{e_i\}$$

The last term in Eqn. 48 is zero, from Eqn. 47. This gives the following result for the change in λ_i with respect to p.

$$\frac{\partial \lambda_i}{\partial p} = \frac{1}{c_i} \lfloor r_i \rfloor \left| \frac{\partial A}{\partial p} \right| \{e_i\} \tag{49}$$

where

$$c_i = \lfloor r_i \rfloor \{e_i\} \neq 0 \tag{50}$$

Equation 49 is an exact solution for the first-order (first derivative) sensitivity of the eigenvalue λ_i to changes in a system parameter, p, present in the $[A_{ij}]$ matrix. Since the matrix $[A_{ij}]$ defined in Eqn. 40 consists of algebraic expressions, we also can derive algebraic expressions for the elements $\frac{\partial A_{ij}}{\partial p}$, as will be illustrated.

We must know $\{r_i\}^T$ and $\{e_i\}$ before we can carry out the operation defined in Eqn. 49. Since the transposed eigenvalue problem is related to the original eigenvalue problem (Eqn. 43), it can be shown that:

$$[R] = [E]^{-1} \tag{51}$$

where the columns of the NxN modal matrix $[E]$ are constructed by inserting the N eigenvectors $\{e_i\}$ such that

$$[E_{ij}] = [\{e_1\}\{e_2\} \ldots \{e_N\}] \tag{51}$$

As a result,

$$[R_{ij}] = \begin{vmatrix} \lfloor r_1 \rfloor \\ \lfloor r_2 \rfloor \\ \cdot \\ \cdot \\ \cdot \\ \lfloor r_N \rfloor \end{vmatrix} \tag{52}$$

and

$$\lfloor r_i \rfloor \{e_i\} = C_i = 1 \qquad (i = 1, 2, \ldots, N) \tag{53}$$

$$\lfloor r_j \rfloor \{e_i\} = 0 \qquad (i \neq j) \tag{54}$$

Since the mode shapes (eigenvectors) of both problems are orthogonal to each other, the sensitivities of all eigenvalues can be computed in a single operation, as follows.

Let us define a matrix $[D_{ij}]$ as follows:

$$[D_{ij}] = [R] \begin{vmatrix} \dfrac{\partial A_{ij}}{\partial p} \end{vmatrix} [E] \tag{55}$$

Then

$$\frac{\partial \lambda_i}{\partial p} = D_{ii} \tag{56}$$

Note that the off-diagonal elements of D_{ij} are not zero, nor are they meaningful.

The procedure for computing sensitivity derivatives of our eigenvalues is now easily constructed.

1. Compute the N eigenvalues and eigenvectors of the problem

$$[\lambda_i[I] - [A]]\{e_i\} = \{0\}$$

2. Construct the matrix $[E_{ij}]$

3. Invert $[E_{ij}]$ to find $[R_{ij}]$

4. Construct the matrix $\left|\dfrac{\partial A_{ij}}{\partial p}\right|$ for the parameter of interest.

5. Compute $[D_{ij}] = [R]\left|\dfrac{\partial A_{ij}}{\partial p}\right|[E]$

6. $\dfrac{\partial \lambda_i}{\partial p} = D_{ii}$

Now, let's turn to the actual computation of the matrix $\left|\dfrac{\partial A}{\partial p}\right|$ for a few parameters. First consider the stiffness cross-coupling parameter ψ.

$$\left[\frac{\partial A_{ij}}{\partial \psi}\right] = \begin{bmatrix} 0 & 0 \\ -M_T^{-1}\dfrac{\partial K_T}{\partial \psi} & 0 \end{bmatrix} \tag{57}$$

The elements of $\left[\dfrac{\partial K_T}{\partial \psi}\right]$ are:

$$\left[\frac{\partial K_T}{\partial \psi}\right] = [K_\psi] = -\frac{1}{\sqrt{R}}\begin{bmatrix} 0 & 1 \\ 1 & 0 \end{bmatrix} \tag{58}$$

Therefore

$$\left[\frac{\partial A_{ij}}{\partial \psi}\right] = \begin{bmatrix} 0 & 0 \\ [-M_T^{-1}][K_\psi] & 0 \end{bmatrix} \tag{59}$$

Next, consider changes with respect to the primary stiffness ratio, R =

K_{11}/K_{22}.

$$\left[\frac{\partial A_{ij}}{\partial R}\right] = \begin{bmatrix} 0 & 0 \\ -M_T^{-1}\frac{\partial K_T}{\partial R} & 0 \end{bmatrix} \tag{60}$$

The elements of $\left[\frac{\partial K_T}{\partial R}\right]$ are:

$$\left[\frac{\partial K_T}{\partial R}\right] = [K_R] = \frac{1}{R}\begin{bmatrix} C & \dfrac{\psi}{2\backslash|\overline{R}} \\ \dfrac{\psi}{2\backslash|\overline{R}} & -1/R \end{bmatrix} \tag{61}$$

Therefore:

$$\left[\frac{\partial A_{ij}}{\partial R}\right] = \begin{bmatrix} 0 & 0 \\ [-M_T]^{-1}[K_R] & 0 \end{bmatrix} \tag{62}$$

It is also important to predict how the eigenvalues change with airspeed since the eigenvalues determine system stability. Let's compute $\left[\dfrac{\partial A_{ij}}{\partial\overline{V}}\right]$, as follows:

$$\left[\frac{\partial A_{ij}}{\partial\overline{V}}\right] = \left[\frac{\partial A_{ij}}{\partial\overline{V}_n}\right]\cos\Lambda \tag{63}$$

and

$$\left[\frac{\partial A_{ij}}{\partial\overline{V}_n}\right] = \begin{bmatrix} 0 & 0 \\ -M_T^{-1}\dfrac{\partial K_T}{\partial\overline{V}_n} & -M_T^{-1}\dfrac{\partial B}{\partial\overline{V}_n} \end{bmatrix} \tag{64}$$

Let us represent the matrix of changes in K_T as

$$\left[\frac{\partial K_T}{\partial\overline{V}_n}\right] = \left[K_{\overline{V}_n}\right] \tag{65}$$

and changes in B_{ij} as

$$\left[\frac{\partial B}{\partial \overline{V}_n}\right] = [B_{\overline{V}_n}]$$ (66)

Elements of these matrices are:

$$K_{\overline{V}_n}(1,1) = \frac{2\overline{V}_n}{d}(-1 + \frac{C_L}{\pi})$$ (67)

$$K_{\overline{V}_n}(1,2) = \frac{-2\overline{V}_n}{d} \tan \Lambda(-1 + \frac{C_L}{\pi})$$ (68)

$$K_{\overline{V}_n}(2,1) = \frac{-2\overline{V}_n}{\pi d} (AR)C(k)C_{1_\alpha}$$ (69)

$$K_{\overline{V}_n}(2,2) = \frac{2\overline{V}_n}{\pi d} (AR)C(k)C_{1_\alpha} \tan \Lambda$$ (70)

Elements of the changes in the aerodynamic damping matrix are:

$$B_{\overline{V}_n}(1,1) = \frac{C_L C_p}{\pi d}$$ (71)

$$B_{\overline{V}_n}(1,2) = (AR + a \tan \Lambda - C_L(AR)/\pi)/d$$ (72)

$$B_{\overline{V}_n}(2,1) = (-AR)(1 - C_{1_\alpha} C_p C(k)/\pi)/d$$ (73)

$$B_{\overline{V}_n}(2,2) = (AR)(\tan \Lambda + \frac{4}{3}C(k)C_{1_\alpha}/\pi)/d$$ (74)

The Addition of a Control Surface to the Idealization

If a full-span, trailing edge control is attached as shown in Figure 4, the equations of motion (Eqn. 36) will be modified. If the control deflection is denoted as δ_o and the control is irreversible, then pitching and bending moments at the airfoil root may be written as:

$$\left\{\begin{array}{c} M_{\theta\delta} \\ M_{\phi\delta} \end{array}\right\} = m r_\alpha^2 \omega_p^2 \left\{\begin{array}{c} \overline{M}_{\theta\delta} \\ \overline{M}_{\phi\delta} \end{array}\right\} \delta_o \tag{75}$$

where

$$\left\{\begin{array}{c} \overline{M}_{\theta\delta} \\ \overline{M}_{\phi\delta} \end{array}\right\} = \frac{2\overline{v}_n^2}{\pi\mu\overline{r}_\alpha^2} \left\{\begin{array}{c} c_{m\delta} + \dfrac{\overline{e}}{2} c_{e\delta} \\ (AR)c1\delta \end{array}\right\} \tag{76}$$

and

$$\overline{e} = a - a_c . \tag{77}$$

Equation 36 now becomes

$$\left[\overline{s}^2 [M_T] + \overline{s}[B] + [K_T]\right]\left\{\begin{array}{c} \theta \\ \phi \end{array}\right\} = \left\{\begin{array}{c} C_{\theta\delta} \\ C_{\phi\delta} \end{array}\right\} \delta_o = \{C_\delta\}\delta_o \tag{78}$$

where

$$c_{\theta\delta} = \frac{2\overline{v}_n^2}{\pi\mu\overline{r}_\alpha^2} (c_{m\delta} + \frac{\overline{e}}{2} C_{1\delta}) \tag{79}$$

and

$$C_{\phi\delta} = \frac{2\overline{v}_n^2}{\pi\mu\overline{r}_\alpha^2} (AR)c_{1\delta} \tag{80}$$

In terms of time derivatives of θ and ϕ, Eqn. 78 is written as:

$$\{\ddot{x}\} = \left\{\begin{array}{c} \ddot{\theta} \\ \ddot{\phi} \end{array}\right\} = -[M_T]^{-1}[K_T]\{x\} - [M_T]^{-1}[B]\{\dot{x}\} + [M_T]^{-1}\{C\delta\}\delta_o \quad (81)$$

Equation 81 may be written in state-space form as:

$$\{\dot{\eta}\} = [A]\{\eta\} + \{B\}\delta_o \quad (82)$$

where

$$\{B\} = \left\{\begin{array}{c} 0 \\ [M_T]^{-1}\{C_\delta\} \end{array}\right\} \quad (83)$$

Note that the symbol [B] also has been used previously to denote for aerodynamic damping. However, in all that follows, the symbol B will refer to the control matrix, in this case, a vector quantity defined in Eqn. 83.

Modal Controllability

The aeroelastic response problem is now cast in terms of the state vector $\{\eta\}$ (defined in Eqn. 41) as follows:

$$\dot{\eta} = A\eta + B\delta \quad . \quad (84)$$

Again, the eigenvectors of the problem $\eta = A\eta$ are $\{e_i\}$ and, as before, can be arranged to form an NxN modal matrix $[E_{ij}]$ defined in Eqn. 51. We can use $[E_{ij}]$ to transform the η coordinates to a new set of coordinates $\{\xi_i\}$, defined as:

$$\{\eta\} = [E_{ij}]\{\xi\} \quad (85)$$

so that

$$\{\xi\} = [E_{ij}]^{-1}\{\eta\} = [R]\{\eta\} \quad (86)$$

Our equation of motion, including the control, then becomes:

$$[E_{ij}]\{\dot{\xi}\} = [A][E_{ij}]\{\xi\} + \{B\}\delta_o \quad (87)$$

or

$$\{\dot{\xi}\} = [R_{ij}][A][E_{ij}]\{\xi\} + [R]\{B\}\delta_o \qquad (88)$$

The matrix RAE = J, is a diagonal matrix composed of the N eigenvalues

of the matrix [A]. The matrix [J] is called the <u>Jordan canonical form</u>

of [A]. Let us define a column matrix {P} as

$$\{P\} = [E_{ij}]^{-1}\{B\} = [R]\{B\} \qquad (89)$$

so that now we have the equation of motion written as:

$$\{\dot{\xi}\} = [J]\{\xi\} + \{P\}\delta_o \qquad (90)$$

The matrix {P} is called the <u>mode-controllability matrix</u> of the system

and has some interesting characteristics.

Since [J] is diagonal and {P} is a vector, the equations of motion

in terms of ξ_i are uncoupled and have the general form:

$$\dot{\xi}_i = \lambda_i \xi_i + P_i \delta_o \qquad (i = 1, 2, \ldots, N) \qquad (91)$$

where λ_i is the ith eigenvalue and ξ_i is the generalized coordinate

corresponding to the ith mode of the system. From this relationship, it

is seen that the ith mode is <u>controllable</u> by the control surface only if

P_i is unequal to zero. The entire system is controllable only if all

modes are controllable.

Mode-observability of the System

The measured "output" of the system can be expressed in terms of

the system states as:

$$\{y\} = [C_{ij}]^T\{\eta\} \qquad (92)$$

where $[C_{ij}]$ represents the system output matrix. In terms of the

transformed coordinates $\{\xi_i\}$, the output equation becomes:

$$\{y\} = [C]^T[E_{ij}]\{\xi\} = [\overline{C}]^T\{\xi\} \tag{93}$$

where

$$[\overline{C}] = [E_{ij}]^T[C] \tag{94}$$

The matrix $[\overline{C}]$ is called the mode-observability matrix for the system.

Modal Control

Only a single control input, δ_o, controls the aerelastic system; let's measure the system states and feedback a signal, f, defined as:

$$f(t) = \{\mu\}^T\{\eta\} \tag{95}$$

The matrix $\{\mu\}$ is a matrix of transducer outputs from each state. This vector $\{\mu\}$ is called the measurement vector. The signal $f(t)$ can be amplified by a _proportional controller_ having a _gain_, K. In this case, the controller is δ_o, so that we move the control surface an amount:

$$\delta_o = K\{\mu\}^T\{\eta\} \tag{96}$$

Combining this with our equation of motion, we now have the following problem.

$$\{\dot{\eta}\} = [A]\{\eta\} + K\{B\}\{\mu\}^T\{\eta\} \tag{97}$$

Let

$$[A_T] = [A] + K\{B\}\{\mu\}^T \tag{98}$$

Then

$$\{\dot{\eta}\} = [A_T]\{\eta\} \tag{99}$$

Depending upon the choice of K and $\{\mu\}$, the eigenvalues of $[A_T]$ will differ from those of the original plant matrix [A]. How one chooses K and $\{\mu\}$ depends upon the objective of the control. Let us suppose that the objective is to modify a single eigenvalue of the original plant.

Let us have as our objective the changing of the jth eigenvalue, λ_j, to a value γ_j while leaving all other values of λ_i ($i \neq j$) of the open-loop system unchanged. Here is one way that this may be done. (Note that what follows is a greatly simplified approach to aeroelastic

control.)

Let $\{\mu\} = \{r_j\}$, the jth eigenvector of the transposed eigenvalue problem. In this case

$$[A_T] = [A] + K\{B\}\{r_j\}^T \tag{101}$$

Now, post-multiply by the kth eigenvector ($k \neq j$) of the open-loop system, $\{e_k\}$, to get:

$$[A_T]\{e_k\} = [A]\{e_k\} + K\{B\}\{r_j\}^T\{e_k\} \tag{102}$$

Because of eigenvector orthogonality, $\{r_j\}^T\{e_k\} = 0$. This leaves

$$[A_T]\{e_k\} = [A]\{e_k\} \tag{103}$$

Since, by definition, $[A]\{e_k\} = \lambda_k\{e_k\}$, Eqn. 103 becomes:

$$[A_T]\{e_k\} \equiv \lambda\{e_k\} \qquad (k \neq j) \tag{104}$$

This last result in Eqn. 104 means that, for this selection of $\{\mu\}$, the eigenvectors and eigenvalues of the closed-loop system (represented by A_T) are identical to those of the uncontrolled, open loop system [A], with the exception of the jth eigenvalue/eigenvector combination. Let's look at this latter combination.

If we now post-multiply Eqn. 101 by $\{e_j\}$ then

$$[A_T]\{e_j\} = [A]\{e_j\} + K\{B\}\{r_j\}^T\{e_j\} \tag{105}$$

or

$$[A_T]\{e_j\} = [A]\{e_j\} + K\{B\} = \lambda_j\{e_j\} + K\{B\} \tag{106}$$

Equation 106 is valid because of orthonormality of the vectors $\{r_j\}$ and $\{e_j\}$ in Eqn. 105. This result implies that, due to feedback control, λ_j is not an eigenvalue of $[A_T]$, nor is $\{e_j\}$ an eigenvector of $[A_T]$.

Since the vector $\{\mu\}$ has been specified, the only unknown in the control law is K, the gain. To determine the value of K necessary to modify λ_i by a certain amount, first remember that p_j is the element of the controllability matrix for the jth mode. It can be shown that, to achieve our objective of eigenvalue modification, we can set the gain K to be:

$$K = (\rho_j - \lambda_j)/p_j \tag{107}$$

where p_j is the element of the controllability matrix related to the jth mode and ρ_j is the new eigenvalue. Notice that the gain K may be complex. This modification procedure is strictly valid only when changing a real eigenvalue λ_j to a real value ρ_j. If λ_i is complex, we need to add an additional step.